Bilal Ashraf et al. *Boundary Value Problems* (2017) 2017:137
DOI 10.1186/s13661-017-0869-7

Boundary Value Problems
a SpringerOpen Journal

RESEARCH Open Access

Mixed convection flow of Casson fluid over a stretching sheet with convective boundary conditions and Hall effect

M Bilal Ashraf[1*], T Hayat[2,3] and A Alsaedi[3]

*Correspondence:
bilalashraf_qau@yahoo.com
[1]Department of Mathematics, COMSATS Institute of Information Technology, Wah Cantt., 47040, Pakistan
Full list of author information is available at the end of the article

Abstract

This learning pacts with the MHD mixed convection flow of Casson fluid over a stretching surface. Examination is achieved in presence of Hall and thermal radiation effects. Heat and mass transfer analysis is deliberated subject to convective boundary conditions. The boundary layer partial differential equations are concentrated into ordinary differential equations via similarity transformations. Series solutions of the causing problems are obtained. The effects of physical parameters on the velocity, temperature and concentration profiles are analyzed and deliberated. Numerical values of skin friction coefficients and local Nusselt and Sherwood numbers for different values of Casson fluid parameter, mixed convection parameter, Hall parameter, Hartman number, radiation parameter and Biot numbers are computed and inspected.

Keywords: Casson fluid; mixed convection flow; thermal radiation; Hall effect; convective boundary conditions

1 Introduction

Recently the flow of an electrically conducting fluid in the presence of magnetic field has had importance in various areas of technology and engineering such as MHD power generation, drawing, annealing, in the purification of molten metals from non-metallic inclusions, electromagnetic pumps, MHD pumps etc. In particular, many metallurgical processes involve the cooling of continuous strips or filaments by drawing through a quiescent fluid. Some-times these strips or filaments are stretched. Actually, the properties of the final product depend upon the rate of cooling in these metallurgical processes. The rate of cooling can be controlled by drawing such strips or filaments in an MHD fluid, which permits to obtain the final product with desired characteristics. The magnetic field can enhance a Lorentz force even in a weak electric current and a magnetization force. It is well known that the influence of Hall current is very important in the presence of a strong magnetic field. In fact, in an ionized gas of low density and/or strong magnetic field, the conductivity normal to the magnetic field decreases by free growth of electrons and ions about the magnetic lines of force before suffering collisions. A current induced in a direction normal to the electric and magnetic fields is called Hall current. Gupta [1] analyzed the hydromagnetic flow past a porous flat plate with Hall effects. Hayat et al. [2]

studied the effects of Hall current and heat transfer on the rotating flow of second grade fluid through a porous medium. Saleem and Aziz [3] explored hydromagnetic flow over a stretching surface with internal heat generation and Hall current. Aziz and Nabil [4] discussed the hydromagnetic mixed convection flow by an exponentially stretching surface with Hall current. Recently Pal [5] analyzed the influence of Hall current and thermal radiation on the unsteady flow of viscous fluid over a permeable stretching surface.

The study of stretching surfaces through various combinations is important in many practical applications. For instance, the production of sheeting material arises in a number of industrial manufacturing processes which include both metal and polymer sheets. After the initial contribution of Crane [6], various researchers extended the flow over a stretching surface in the directions of Newtonian and non-Newtonian fluid models under different geometries. The Casson fluid model is one of the non-Newtonian fluid models which reveal the characteristics of yield stress. Also Casson fluid acts like a solid when the shear stress less than the yield stress is applied, and it moves if the applied shear stress is greater than the yield stress. Jelly, soup, honey, tomato sauce, concentrated fruit juices and many others are the examples of Casson fluid. Some relevant studies about this fluid model can be seen in the refs [7–10].

Thermal and concentration convections in the boundary layer flow over a stretching surface subject to constant but different temperatures and concentrations at the boundaries have been considered extensively by the researchers. Such flows occur in a number of engineering, geophysical and energy storage applications. In nature most of the problems dealing with flow over a moving surface are developed by the movement of the boundary and buoyancy effects through thermal and concentration convections. Practical examples of such flows are solar central receivers exposed to wind currents, electronic devices cooled by fans, nuclear reactors cooled during emergency shutdown etc. The problem of steady laminar hydromagnetic heat transfer in the mixed convection flow by a vertical plate embedded in a uniform porous medium was studied by Makinde and Sibanda [11]. Turkyilmazoglu [12] constructed the analytical solution of mixed convection flow of MHD viscoelastic fluid over a permeable stretching surface. Recently Alsaadi et al. [13] studied the mixed convection flow of second grade fluid bounded by a permeable stretching surface with Soret and Dufour effects. Note that the aforementioned research disregarded the radiation effects. However, the technological processes at high temperatures involve the thermal radiation heat transfer. For example, in hypersonic flights, missile reentry rocket combustion chambers, gas cooled nuclear reactors and power plants for inter-planetary flight, the attention of researchers was focused on thermal radiation as a mode of energy transfer, and they emphasized the need for discussion on inclusion of radiative transfer in these processes [14, 15]. Mukhopadhyay [16] investigated the effects of thermal radiation in the unsteady boundary layer mixed convection flow by a vertical permeable stretching surface embedded in a porous medium. The fluid is assumed viscous and incompressible. Turkyilmazoglu [17] considered the impact of thermal radiation on the unsteady laminar convective MHD temperature-dependent viscosity flow over a rotating porous disk. Shehzad et al. [18] presented the magnetohydrodynamic (MHD) radiative flow of an incompressible Jeffrey fluid over a linearly stretched surface with Joule heating and thermophoretic effects. Recently Aziz [19] used the model of convective boundary condition for the investigation of Blasius flow. Some studies relevant to convective conditions can be read in the attempts [20–22].

The aim of present investigation is to study the Hall effects on the flow of Casson fluid in presence of thermal radiation and mixed convection. Convective heat and mass transfer at the boundaries is also considered. To our knowledge, there is no such study available in the literature. The resulting boundary layer partial differential equations are transformed into ordinary differential equations. Convergence criteria of series solutions are given by using the homotopy analysis method [23–30]. Impacts of embedding parameters on the flow, temperature and concentration fields are examined graphically. Numerical values of skin friction coefficient, transversal skin friction coefficient, local Nusselt and Sherwood numbers for secondary variables are obtained and discussed.

2 Mathematical modeling

Consider the mixed convection boundary layer flow of Casson fluid over a stretching surface in presence of thermal radiation. A uniform magnetic field B_0 is imposed along the normal direction to a stretching surface. The effect of Hall current is taken into account. Heat and mass transfer in presence of convective boundary conditions is considered.

Generalized Ohms' law may be put in the form

$$\mathbf{J} = \frac{\sigma}{1+m^2}\left(\mathbf{E} + \mathbf{V}\times\mathbf{B} - \frac{1}{en_e}\mathbf{J}\times\mathbf{B}\right), \tag{1}$$

where $\mathbf{V}$ is the velocity vector, $\mathbf{E}$ is the intensity vector of the electric field, $\mathbf{B}$ is the magnetic induction vector, $\mathbf{J}$ is the electric current density vector, $m = (\frac{\sigma B_0}{en_e})$ is the Hall parameter, σ is the electrical conductivity, e is the charge of electron and n_e is the number density of electron. Hall current produces a force in z-direction which generates a cross flow velocity in this direction, and thus the flow becomes three dimensional.

The velocity field is taken as follows:

$$\mathbf{V} = \big[u(x,y), v(x,y), 0\big], \tag{2}$$

where u and v denote the velocity components in the x- and y-directions.

The governing equations for the flow can be expressed as

$$\frac{\partial u}{\partial x} + \frac{\partial v}{\partial y} + \frac{\partial w}{\partial z} = 0, \tag{3}$$

$$u\frac{\partial u}{\partial x} + v\frac{\partial u}{\partial y} = \nu\left(1+\frac{1}{\beta}\right)\frac{\partial^2 u}{\partial y^2} + g\beta_T(T-T_\infty) + g\beta_C(C-C_\infty) - \frac{\sigma^* B_0^2}{\rho(1+m^2)}(u+mw), \tag{4}$$

$$u\frac{\partial w}{\partial x} + v\frac{\partial w}{\partial y} = \nu\left(1+\frac{1}{\beta}\right)\frac{\partial^2 w}{\partial y^2} + \frac{\sigma^* B_0^2}{\rho(1+m^2)}(mu-w), \tag{5}$$

$$u\frac{\partial T}{\partial x} + v\frac{\partial T}{\partial y} = \alpha\frac{\partial^2 T}{\partial y^2} - \frac{1}{\rho c_p}\frac{\partial q_r}{\partial y}, \tag{6}$$

$$u\frac{\partial C}{\partial x} + v\frac{\partial C}{\partial y} = D_B\frac{\partial^2 C}{\partial y^2}, \tag{7}$$

where u, v and w are the velocity components in the x-, y- and z-directions, respectively, β is the Casson fluid parameter, β_T is the thermal expansion coefficient, β_C is the concen-

tration expansion coefficient, σ^* is the electrical conductivity, ρ is the density of fluid, g is the gravitational acceleration, $\nu = (\mu_B/\rho)$ is the kinematic viscosity, α is the thermal diffusivity of fluid, T is the fluid temperature, C is the concentration field and D is the mass diffusivity.

The radiative heat flux q_r through Rosseland approximations is given by [16–18]

$$q_r = -\frac{4\sigma_s}{3k_e}\frac{\partial T^4}{\partial y}, \tag{8}$$

where σ_s is the Stefan-Boltzmann constant and k_e is the mean absorption coefficient. If the temperature differences are sufficiently small, then Eq. (6) can be linearized by expanding T^4 into the Taylor series about T_∞ which, after neglecting higher order terms, takes the form

$$T^4 = 4T_\infty^3 T - 3T_\infty^4. \tag{9}$$

By using Eqs. (8) and (9), Eq. (6) reduces to

$$u\frac{\partial T}{\partial x} + \nu\frac{\partial T}{\partial y} = \alpha\frac{\partial^2 T}{\partial z^2} - \frac{16\sigma_s T_\infty^3}{3k_e\rho c_p}\frac{\partial^2 T}{\partial y^2}. \tag{10}$$

The boundary conditions are

$$\begin{aligned} &u = U_w(x) = cx, \qquad \nu = 0, \qquad -k\frac{\partial T}{\partial y} = h_1(T_f - T),\\ &-D\frac{\partial C}{\partial y} = h_2(C_f - C) \quad \text{at } y = 0, \end{aligned} \tag{11}$$

$$u \to 0, \qquad \nu \to 0, \qquad T \to T_\infty, \qquad C \to C_\infty \quad \text{as } y \to \infty, \tag{12}$$

where subscript w corresponds to the wall condition, h_1 is the heat transfer coefficient, h_2 is the mass transfer coefficient, T_f is the fluid temperature and C_f is the fluid concentration.

Considering

$$\begin{aligned} &\eta = y\sqrt{\frac{c}{\nu}}, \qquad u = cxf'(\eta), \qquad \nu = -\sqrt{c\nu}f(\eta), \qquad w = cxh(\eta),\\ &\theta(\eta) = \frac{T - T_\infty}{T_f - T_\infty}, \qquad \varphi(\eta) = \frac{C - C_\infty}{C_w - C_\infty}, \end{aligned} \tag{13}$$

Eq. (1) is identically satisfied and Eqs. (4)-(10) can be converted to the following forms:

$$\left(1 + \frac{1}{\beta}\right)f''' + ff'' - \left(f'\right)^2 + \lambda(\theta + N\varphi) - \frac{M}{1 + m^2}\left(f' + mh\right) = 0, \tag{14}$$

$$\left(1 + \frac{1}{\beta}\right)h'' + fh' - \left(f' + \frac{M}{1 + m^2}\right)h + \frac{M}{1 + m^2}mf' = 0, \tag{15}$$

$$\left(1 + \frac{4}{3}R\right)\theta'' + \Pr f\theta' = 0, \tag{16}$$

$$\varphi'' + Scf\varphi' = 0, \tag{17}$$

$$f = h = 0, \qquad f' = 1, \qquad \theta' = -\gamma_1\big(1-\theta(0)\big), \qquad \varphi' = -\gamma_2\big(1-\varphi(0)\big), \quad \text{at } \eta = 0, \tag{18}$$

$$f' \to 0, \qquad h \to 0, \qquad \theta \to 0, \qquad \varphi \to 0 \quad \text{as } \eta \to \infty, \tag{19}$$

where λ is the mixed convection parameter, Gr_x is the local Grashof number, N is the concentration buoyancy parameter, M is the Hartman number, R is the radiation parameter, Pr is the Prandtl number, Sc is the Shmidt number, γ_1 is the heat transfer Biot number and γ_2 is the mass transfer Biot number. These can be defined as follows:

$$\begin{aligned}
&\lambda = \frac{\mathrm{Gr}_x}{\mathrm{Re}_x^2}, \qquad \mathrm{Gr}_x = \frac{g\beta_T(T_f - T_\infty)x^3}{\upsilon^2}, \qquad N = \frac{\beta_C(C_f - C_\infty)}{\beta_T(T_f - T_\infty)},\\
&R = \left(\frac{4\sigma^* T_\infty^3}{k_e k}\right), \qquad M = \frac{\sigma^* B_0^2}{\rho},\\
&\mathrm{Pr} = \frac{\nu}{\sigma}, \qquad \mathrm{Sc} = \frac{\nu}{D}, \qquad \gamma_1 = \frac{h_1}{k}\sqrt{\frac{\nu}{a}}, \qquad \gamma_2 = \frac{h_2}{D}\sqrt{\frac{\nu}{a}}.
\end{aligned} \tag{20}$$

Non-dimensional local skin friction coefficients and local Nusselt and Sherwood numbers are

$$\frac{1}{2}C_f\mathrm{Re}_x^{1/2} = -(1+1/\beta)f''(0), \tag{21}$$

$$\frac{1}{2}C_f\mathrm{Re}_x^{1/2} = -(1+1/\beta)h'(0), \tag{22}$$

$$Nu/\mathrm{Re}_x^{1/2} = -\theta'(0), \tag{23}$$

$$Sh/\mathrm{Re}_x^{1/2} = -\varphi'(0), \tag{24}$$

in which $\mathrm{Re}_x = \frac{cx}{\nu}$ is the local Reynold number.

3 Series solutions

Initial guesses and auxiliary linear operators for series solutions are chosen in the forms

$$\begin{aligned}
&f_0(\eta) = \big(1 - e^{-\eta}\big), \qquad h_0(\eta) = 0,\\
&\theta_0(\eta) = \frac{\gamma_1 \exp(-\eta)}{1+\gamma_1}, \qquad \varphi_0(\eta) = \frac{\gamma_2 \exp(-\eta)}{1+\gamma_2},
\end{aligned} \tag{25}$$

$$L_f = f'''' - f', \qquad L_h = h'' - h, \qquad L_\theta = \theta'' - \theta, \qquad L_\varphi = \varphi'' - \varphi, \tag{26}$$

with the following properties:

$$\begin{aligned}
&L_f\big(C_1 + C_2 e^{\eta} + C_3 e^{-\eta}\big) = 0, \qquad L_h\big(C_4 e^{\eta} + C_5 e^{-\eta}\big) = 0,\\
&L_\theta\big(C_6 e^{\eta} + C_7 e^{-\eta}\big) = 0, \qquad L_\varphi\big(C_8 e^{\eta} + C_9 e^{-\eta}\big) = 0,
\end{aligned} \tag{27}$$

where C_i (i = 1-9) are the arbitrary constants.

The zeroth order deformation problems are given by

$$(1-p)L_f\big[\hat{f}(\eta;p) - f_0(\eta)\big] = p\hbar_f \mathbf{N}_f\big[\hat{f}(\eta;p), \hat{h}(\eta;p), \hat{\theta}(\eta;p), \hat{\varphi}(\eta;p)\big], \tag{28}$$

$$(1-p)L_f\big[\hat{h}(\eta;p)-h_0(\eta)\big]=p\hbar_h\mathbf{N}_h\big[\hat{h}(\eta;p),\hat{f}(\eta;p),\hat{\theta}(\eta;p),\hat{\varphi}(\eta;p)\big], \tag{29}$$

$$(1-p)L_\theta\big[\hat{\theta}(\eta;p)-\theta_0(\eta)\big]=p\hbar_\theta\mathbf{N}_\theta\big[\hat{f}(\eta;p),\hat{\theta}(\eta;p)\big], \tag{30}$$

$$(1-p)L_\varphi\big[\hat{\varphi}(\eta;p)-\varphi_0(\eta)\big]=p\hbar_\varphi\mathbf{N}_\varphi\big[\hat{f}(\eta;p),\hat{\theta}(\eta;p)\big], \tag{31}$$

$$\begin{aligned}&\hat{f}(0;p)=0,\qquad \hat{f}'(0;p)=1,\qquad \hat{f}'(\infty;p)=0,\qquad \hat{h}(0;p)=0,\qquad \hat{h}(\infty;p)=0,\\&\hat{\theta}'(0,p)=-\gamma_1\big[1-\theta(0,p)\big],\qquad \hat{\theta}(\infty,p)=0,\qquad \hat{\varphi}'(0,p)=-\gamma_2\big[1-\hat{\varphi}(0,p)\big],\\&\hat{\varphi}(\infty,p)=0,\end{aligned} \tag{32}$$

$$\begin{aligned}&\mathbf{N}_f\big[\hat{f}(\eta;p),\hat{h}(\eta;p),\hat{\theta}(\eta;p),\hat{\varphi}(\eta;p)\big]\\&\quad=\left(1+\frac{1}{\beta}\right)\frac{\partial^3\hat{f}(\eta,p)}{\partial\eta^3}+\hat{f}(\eta,p)\frac{\partial^2\hat{f}(\eta,p)}{\partial\eta^2}-\left(\frac{\partial\hat{f}(\eta,p)}{\partial\eta}\right)^2\\&\qquad+\lambda\begin{pmatrix}\hat{\theta}(\eta,p)\\+N\hat{\varphi}(\eta;p)\end{pmatrix}-\frac{M}{1+m^2}\begin{pmatrix}\frac{\partial\hat{f}(\eta,p)}{\partial\eta}\\+m\hat{h}(\eta,p)\end{pmatrix},\end{aligned} \tag{33}$$

$$\begin{aligned}\mathbf{N}_h\big[\hat{h}(\eta;p),\hat{f}(\eta;p)\big]&=\left(1+\frac{1}{\beta}\right)\frac{\partial^2\hat{h}(\eta;p)}{\partial\eta^2}+\hat{f}(\eta,p)\frac{\partial\hat{h}(\eta;p)}{\partial\eta}-\begin{pmatrix}\frac{\partial\hat{f}(\eta,p)}{\partial\eta}\\+\frac{M}{1+m^2}\end{pmatrix}\hat{h}(\eta;p)\\&\quad+\frac{Mm}{1+m^2}\frac{\partial\hat{f}(\eta,p)}{\partial\eta},\end{aligned} \tag{34}$$

$$\mathbf{N}_\theta\big[\hat{f}(\eta;p),\hat{\theta}(\eta;p)\big]=\left(1+\frac{4}{3}R\right)\frac{\partial^2\hat{\theta}(\eta,p)}{\partial\eta^2}+\Pr(\hat{f}(\eta,p)\frac{\partial\hat{\theta}(\eta,p)}{\partial\eta}, \tag{35}$$

$$\mathbf{N}_\varphi\big[\hat{f}(\eta;p),\hat{\theta}(\eta;p)\big]=\frac{\partial^2\hat{\varphi}(\eta;p)}{\partial\eta^2}+\mathrm{Sc}\hat{f}(\eta,p)\frac{\partial\hat{\varphi}(\eta;p)}{\partial\eta}. \tag{36}$$

In the above expressions, p is an embedding parameter, $\hbar_f$, $\hbar_h$, $\hbar_\theta$ and $\hbar_\varphi$ are the non-zero auxiliary parameters and $\mathbf{N}_f$, $\mathbf{N}_h$, $\mathbf{N}_\theta$ and $\mathbf{N}_\varphi$ are the nonlinear operators. Taking $p=0$ and $p=1$, we have

$$\begin{aligned}&\hat{f}(\eta;0)=f_0(\eta),\qquad \hat{h}(\eta;0)=h_0(\eta),\qquad \hat{\theta}(\eta,0)=\theta_0(\eta),\qquad \hat{\varphi}(\eta;0)=\varphi_0(\eta),\\&\hat{f}(\eta;1)=f(\eta),\qquad \hat{h}(\eta;1)=h(\eta),\qquad \hat{\theta}(\eta,1)=\theta(\eta),\qquad \hat{\varphi}(\eta;1)=\varphi(\eta).\end{aligned} \tag{37}$$

When p varies from 0 to 1, then $f(\eta,p)$, $h(\eta,p)$, $\theta(\eta,p)$ and $\varphi(\eta,p)$ differ from $f_0(\eta)$, $h_0(\eta)$, $\theta_0(\eta)$ and $\varphi_0(\eta)$ to $f(\eta)$, $h(\eta)$, $\theta(\eta)$ and $\varphi(\eta)$. Using Taylor series expansion, we obtain

$$f(\eta,p)=f_0(\eta)+\sum_{m=1}^{\infty}f_m(\eta)p^m,\qquad f_m(\eta)=\frac{1}{m!}\frac{\partial^m f(\eta;p)}{\partial p^m}\bigg|_{p=0}, \tag{38}$$

$$h(\eta,p)=h_0(\eta)+\sum_{m=1}^{\infty}h_m(\eta)p^m,\qquad h_m(\eta)=\frac{1}{m!}\frac{\partial^m h(\eta;p)}{\partial p^m}\bigg|_{p=0}, \tag{39}$$

$$\theta(\eta,p)=\theta_0(\eta)+\sum_{m=1}^{\infty}\theta_m(\eta)p^m,\qquad \theta_m(\eta)=\frac{1}{m!}\frac{\partial^m\theta(\eta;p)}{\partial p^m}\bigg|_{p=0}, \tag{40}$$

$$\varphi(\eta,p)=\varphi_0(\eta)+\sum_{m=1}^{\infty}\varphi_m(\eta)p^m,\qquad \varphi_m(\eta)=\frac{1}{m!}\frac{\partial^m\varphi(\eta;p)}{\partial p^m}x\bigg|_{p=0}. \tag{41}$$

The convergence of the above series strongly depends upon $\hbar_f$, $\hbar_h$, $\hbar_\theta$ and $\hbar_\varphi$. Considering that $\hbar_f$, $\hbar_h$, $\hbar_\theta$ and $\hbar_\varphi$ are selected properly so that Eqs. (38)-(41) converge at $p = 1$, we have

$$f(\eta) = f_0(\eta) + \sum_{m=1}^{\infty} f_m(\eta), \tag{42}$$

$$h(\eta) = h_0(\eta) + \sum_{m=1}^{\infty} h_m(\eta), \tag{43}$$

$$\theta(\eta) = \theta_0(\eta) + \sum_{m=1}^{\infty} \theta_m(\eta), \tag{44}$$

$$\varphi(\eta) = \varphi_0(\eta) + \sum_{m=1}^{\infty} \varphi_m(\eta). \tag{45}$$

The problems corresponding to the mth order are

$$L_f\big[f_m(\eta) - \chi_m f_{m-1}(\eta)\big] = \hbar_f \mathbf{R}_f^m(\eta), \tag{46}$$

$$L_h\big[h_m(\eta) - \chi_m h_{m-1}(\eta)\big] = \hbar_h \mathbf{R}_h^m(\eta), \tag{47}$$

$$L_\theta\big[\theta_m(\eta) - \chi_m \theta_{m-1}(\eta)\big] = \hbar_\theta \mathbf{R}_\theta^m(\eta), \tag{48}$$

$$L_\varphi\big[\varphi_m(\eta) - \chi_m \varphi_{m-1}(\eta)\big] = \hbar_\varphi \mathbf{R}_\varphi^m(\eta), \tag{49}$$

$$\begin{aligned} &f_m(0) = f_m'(0) = f_m'(\infty) = h_m(0) = h_m(\infty) = 0, \\ &\theta_m'(0) - \gamma\theta_m(0) = \theta_m(\infty) = 0, \qquad \varphi_m'(0) - \gamma_1\varphi_m(0) = \varphi_m(\infty) = 0, \end{aligned} \tag{50}$$

$$\begin{aligned} \mathbf{R}_f^m(\eta) = {} & f_{m-1}'''(\eta) - \sum_{k=0}^{m-1} f_{m-1-k}' f_k' + \sum_{k=0}^{m-1} f_{m-1-k} f_k'' - \frac{M}{1+m^2} \begin{pmatrix} f_{m-1}'(\eta) \\ + m h_{m-1}(\eta) \end{pmatrix} \\ & + \lambda(\theta + N\varphi), \end{aligned} \tag{51}$$

$$\mathbf{R}_h^m(\eta) = h_{m-1}''(\eta) + \sum_{k=0}^{m-1} f_{m-1-k} h_k' - \sum_{k=0}^{m-1} f_{m-1-k}' h_k - \frac{M}{1+m^2}(h_{m-1}(\eta) - m f_{m-1}'(\eta), \tag{52}$$

$$\mathbf{R}_\theta^m(\eta) = \left(1 + \frac{4}{3}R\right)\theta_{m-1}'' + \Pr \sum_{k=0}^{m-1} \big(\theta_{m-1-k}' f_k\big), \tag{53}$$

$$\mathbf{R}_\varphi^m(\eta) = \varphi_{m-1}'' + \mathrm{Sc} \sum_{k=0}^{m-1} \big(\varphi_{m-1-k}' f_k\big). \tag{54}$$

Solving the mth order deformation problems, we have

$$f_m(\eta) = f_m^*(\eta) + C_1 + C_2 e^{\eta} + C_3 e^{-\eta}, \tag{55}$$

$$h_m(\eta) = h_m^*(\eta) + C_4 e^{\eta} + C_5 e^{-\eta}, \tag{56}$$

$$\theta_m(\eta) = \theta_m^*(\eta) + C_6 e^{\eta} + C_7 e^{-\eta}, \tag{57}$$

$$\varphi_m(\eta) = \varphi_m^*(\eta) + C_8 e^{\eta} + C_9 e^{-\eta}, \tag{58}$$

where the special solutions are f_m^*, h_m^*, θ_m^* and φ_m^*.

4 Convergence analysis and discussion

It is obvious that the series solutions (42)-(45) depend on the auxiliary parameters $\hbar_f$, $\hbar_h$, $\hbar_\theta$ and $\hbar_\varphi$. The proper values of these auxiliary parameters are essential in order to adjust and control the convergence of the series solutions. We have sketched the $\hbar$-curves at 15th order of approximations to determine the convergence region. It is noticed that an appropriate range of auxiliary parameters $\hbar_f$, $\hbar_h$, $\hbar_\theta$ and $\hbar_\varphi$ is $-0.4 \leq \hbar_f \leq -0.10$, $-0.5 \leq \hbar_h \leq -0.05$, $-0.6 \leq \hbar_\theta \leq -0.10$ and $-0.6 \leq \hbar_\theta \leq -0.20$ (see Figure 1). Table 1 ensures that the series solutions converge in the whole region of η when $\hbar_f = \hbar_h = \hbar_\theta = \hbar_\varphi = -0.3$.

The effects of Casson parameter β, Hartman number M, mixed convection parameter λ and concentration buoyancy parameter N on the velocity profile $f'(\eta)$ are examined in Figures 2-5. Figure 2 shows that the velocity profile $f'(\eta)$ and momentum boundary layer thickness decrease with an increase in Casson parameter β. Variation of Hartman number M on the velocity profile $f'(\eta)$ is depicted in Figure 3. It is found that an increase in M leads to a decrease in the velocity profile $f'(\eta)$ and momentum boundary layer thickness. This is due to the fact that an increase in M gives rise to the Lorentz force which resists the flow. The effects of mixed convection parameter λ on the velocity profile $f'(\eta)$ in both assisting and opposing flows are analyzed in Figure 4. It is observed that the velocity profile $f'(\eta)$ and momentum boundary layer thickness are enhanced when $\lambda > 0$ (assisting flow), while opposite behavior is noted for $\lambda < 0$ (opposing flow). For the case of assisting flow the buoyancy forces are more dominant than viscous forces, while an opposite situation occurred in the case of opposing flow. Figure 5 displays that an enhancement in N leads to an increase in momentum boundary layer thickness and velocity profile $f'(\eta)$.

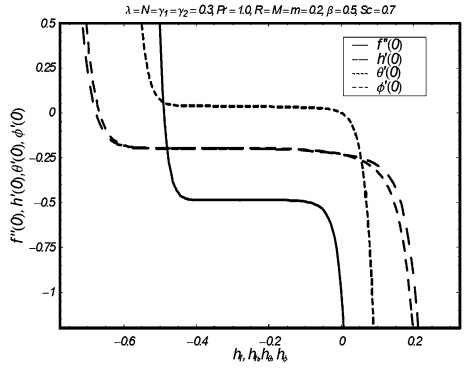

Figure 1 $\hbar$**-curves for the functions** f, h, θ **and** φ.

Table 1 Merging of series results for altered order of calculations when $\beta = m = 0.5$, $\lambda = N = R = 0.3$, $M = \gamma_1 = \gamma_2 = 0.2$, Pr = 1.0, Sc = 0.7 and $\hbar_f = \hbar_w = \hbar_\theta = \hbar_\varphi = -0.3$

Order of approximations	$-f''(0)$	$h'(0)$	$-\theta'(0)$	$-\varphi'(0)$
1	0.70525	0.015000	0.16222	0.16347
5	0.58605	0.027872	0.15239	0.15513
10	0.57654	0.030466	0.14810	0.15009
15	0.57496	0.031056	0.14688	0.14782
20	0.57468	0.031221	0.14661	0.14682
25	0.57466	0.031273	0.14659	0.14639
30	0.57467	0.031292	0.14662	0.14622
35	0.57467	0.031299	0.14663	0.14616
40	0.57467	0.031299	0.14663	0.14616

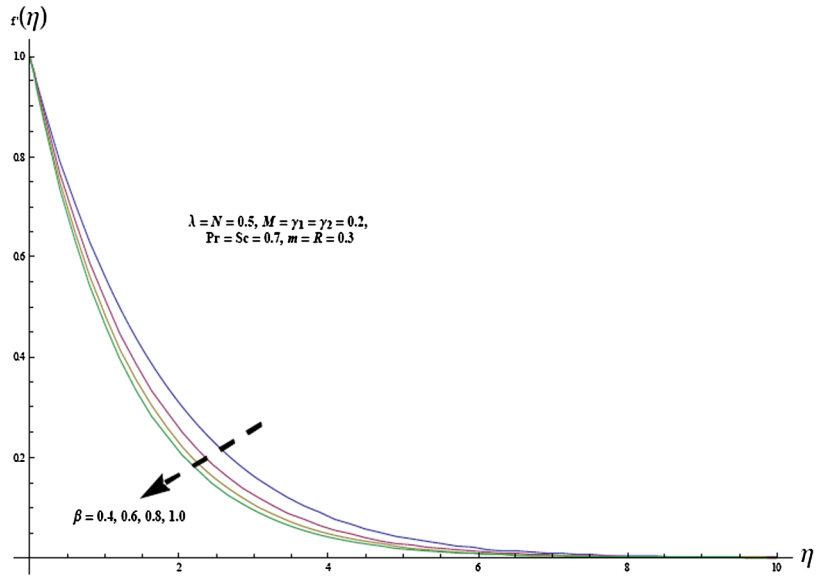

Figure 2 Variation of β on $f'(\eta)$.

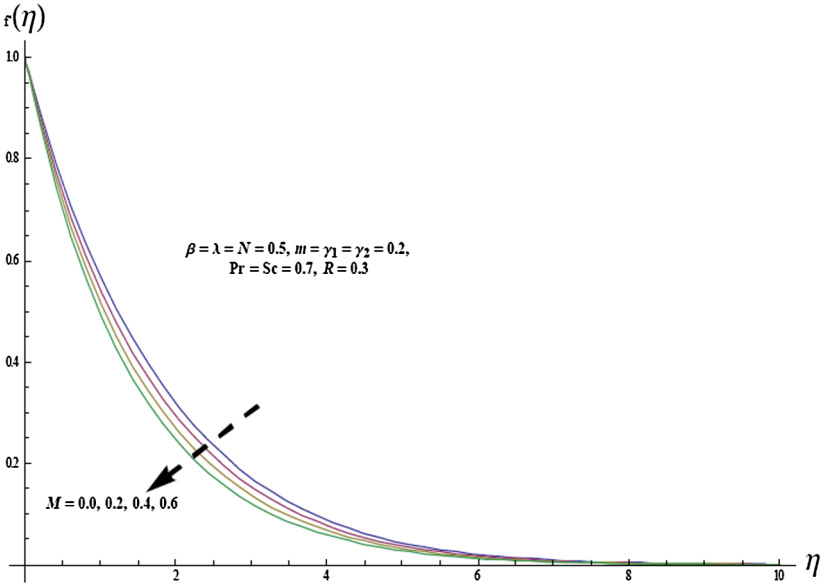

Figure 3 Variation of M on $f'(\eta)$.

The impacts of Hartman number M, Hall parameter m, mixed convection parameter λ and concentration buoyancy parameter N on the transverse velocity profile $h(\eta)$ are depicted in Figures 6-9. Figure 6 shows that the transverse velocity $h(\eta)$ increases with an increase in Hartman number M. It is also noticed that the momentum boundary layer thickness reduces for larger M. The effect of Hall parameter m on the transverse velocity $h(\eta)$ is displayed in Figure 7. As Hall parameter m increases, the transverse velocity $h(\eta)$ decreases and the associated boundary layer thickness increases. The effect of mixed convection parameter λ on the transverse velocity profile $h(\eta)$ is analyzed in Figure 8.

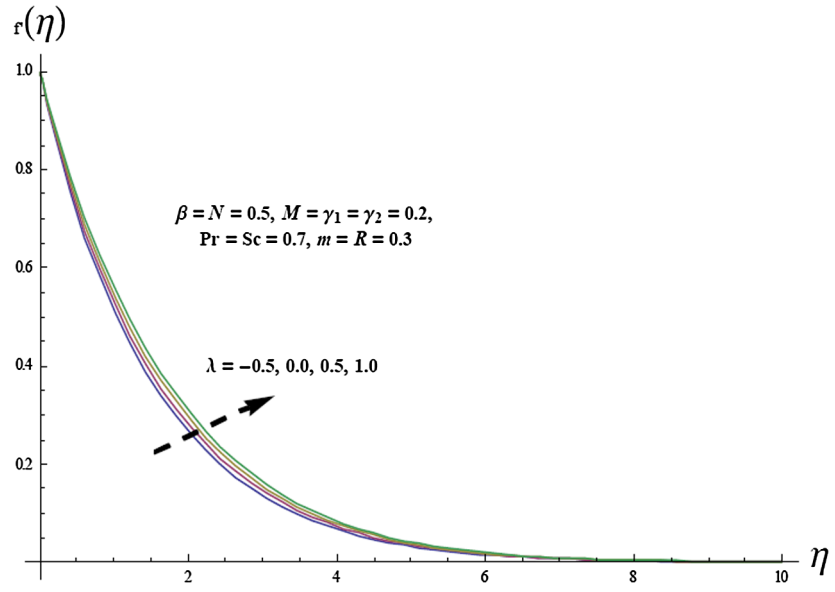

Figure 4 Variation of λ on $f'(\eta)$.

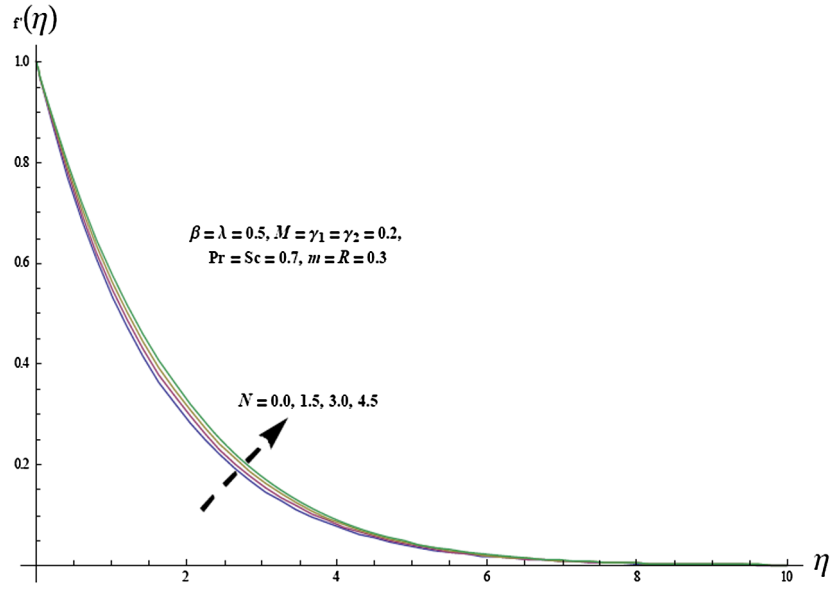

Figure 5 Variation of *N* on $f'(\eta)$.

In the case of assisting flow ($\lambda > 0$) transverse velocity profile $h(\eta)$ enhances. It is due to the fact that viscous forces reduce in the case of assisting flow. Also momentum boundary layer thickness reduces near the stretching surface, while it enhances far away from the sheet. Reverse behavior is noted in the case of opposing flow ($\lambda < 0$). The influence of concentration buoyancy parameter N on the transverse velocity profile $h(\eta)$ is seen in Figure 9. Transverse velocity $h(\eta)$ increases near the surface, and it decreases far away from the surface. The boundary layer thickness reduces near the surface, while it increases far away from the surface.

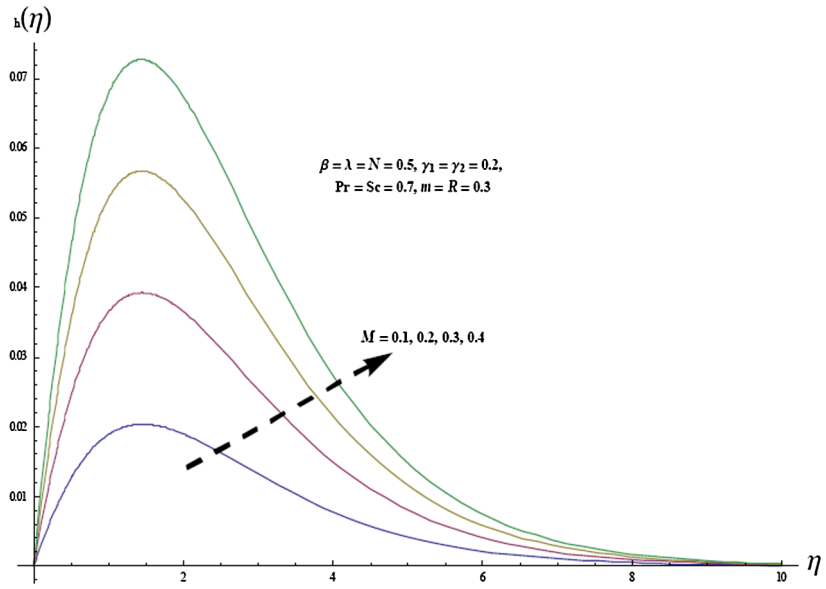

Figure 6 Variation of M on $h(\eta)$.

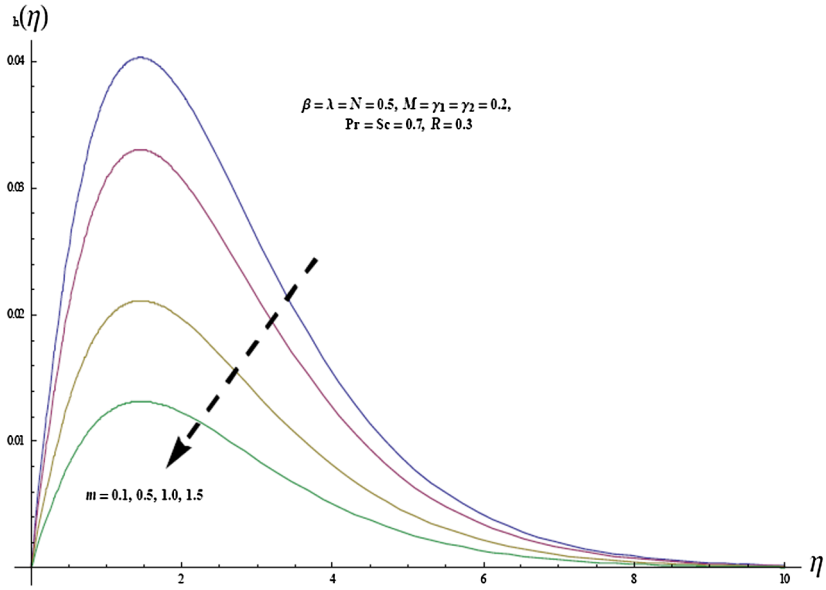

Figure 7 Variation of m on $h(\eta)$.

Figures 10-12 are displayed to see the variations of Biot number γ_1, radiation parameter R and Prandtl number Pr on the temperature $\theta(\eta)$. Figure 10 exhibits that thermal boundary layer thickness and temperature $\theta(\eta)$ are enhanced by increasing γ_1. In fact an increase in Biot number γ_1 corresponds to the larger heat transfer coefficient which increases the thermal boundary layer thickness. Variation of radiation parameter R on the temperature $\theta(\eta)$ and thermal boundary layer thickness is depicted in Figure 11. Here an increase in R leads to rise in the temperature and thermal boundary layer thickness. This is because of the fact that an increase in thermal radiation parameter reduces the mean

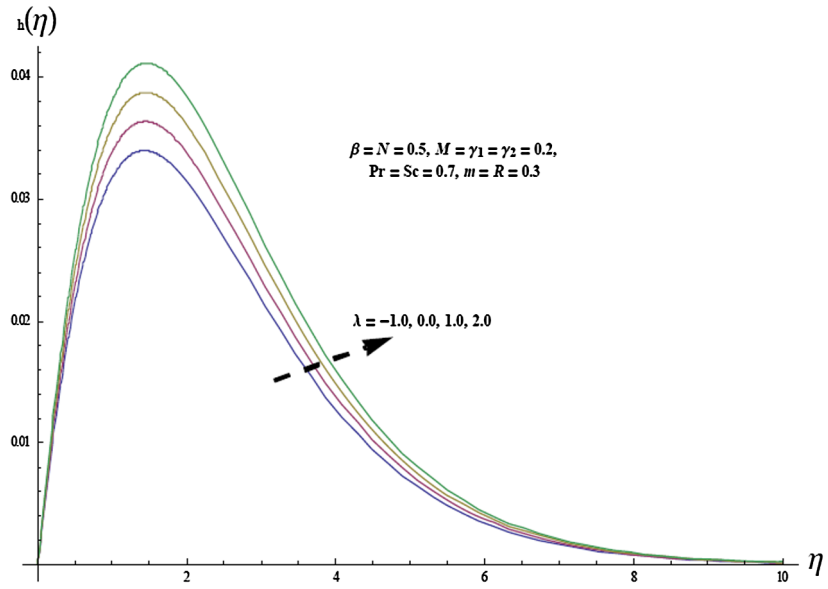

Figure 8 Variation of λ on $h(\eta)$.

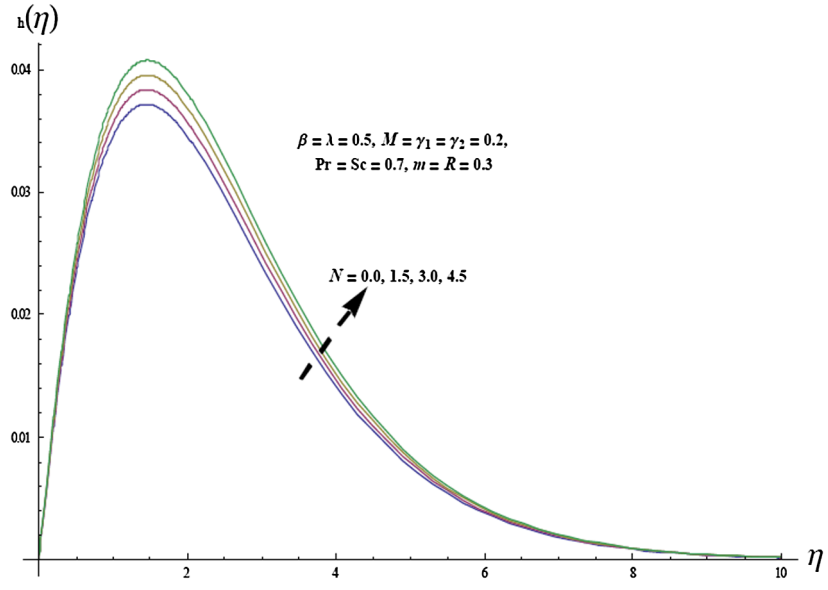

Figure 9 Variation of N on $h(\eta)$.

absorption coefficient k_e, due to which the divergence of the radiative heat flux enhances. Hence the rate of radiative heat transferred to the fluid will be enhanced, and consequently the fluid temperature will increase. Figure 12 displays the effect of Prandtl number Pr on the temperature $\theta(\eta)$. An enhancement in Pr reduces the thermal diffusivity, which shows a decrease in the temperature $\theta(\eta)$ and thermal boundary layer thickness.

The effects of Biot number γ_2, Schmidt number Sc and Hall parameter m on the concentration profile $\varphi(\eta)$ are drawn in Figures 13-15. Mass transfer coefficient enhances when we increase γ_2. Such an enhancement in mass transfer coefficient yields an increase in $\varphi(\eta)$

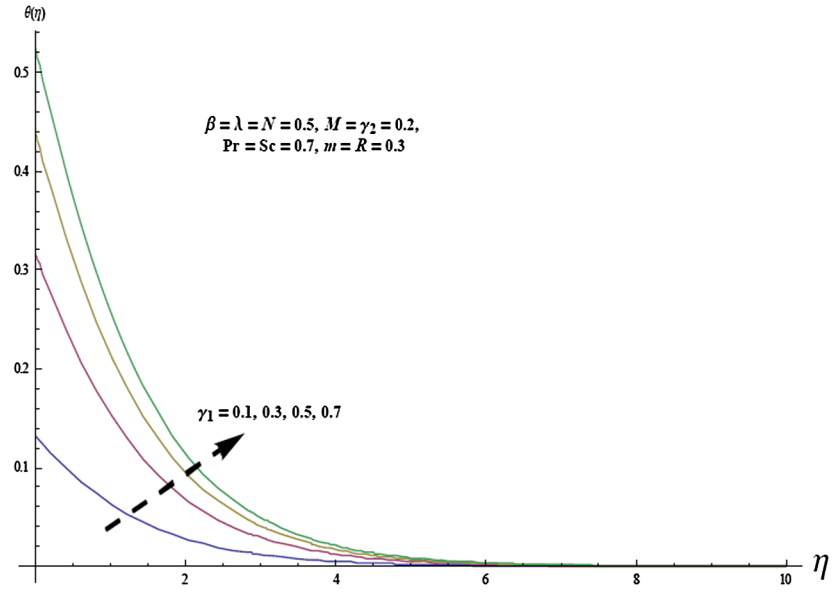

Figure 10 Variation of γ_1 on $\theta(\eta)$.

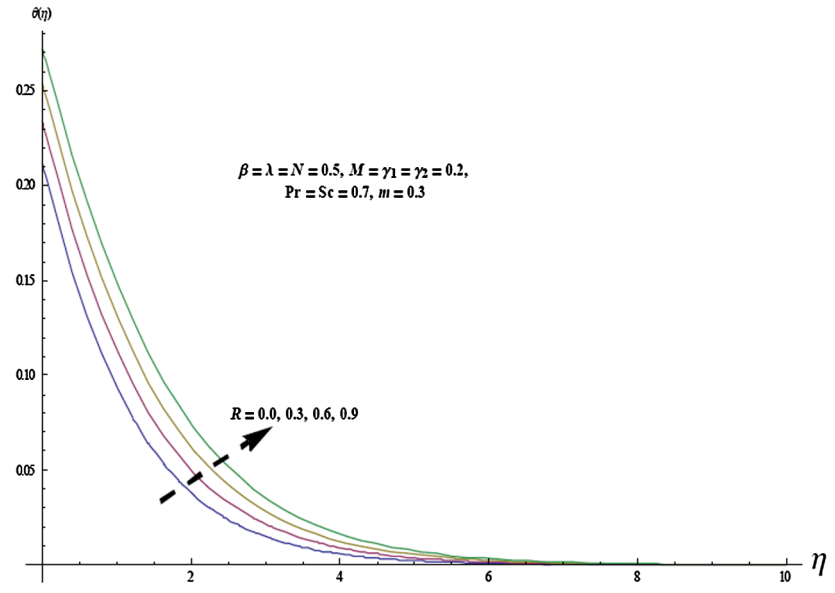

Figure 11 Variation of R on $\theta(\eta)$.

and its associated boundary layer thickness (see Figure 13). Figure 14 depicts the effect of Sc on the concentration profile $\varphi(\eta)$. With an enhancement in Sc, the mass diffusivity reduces and thus concentration profile $\varphi(\eta)$ decreases. Figure 15 shows that concentration profile $\varphi(\eta)$ reduces for larger Hall parameter m. Also the associated boundary layer thickness decreases when m increases.

Table 2 is prepared to see the numerical values of skin friction coefficients, local Nusselt and Sherwood numbers for different values of Casson fluid parameter β, Hartman number M, mixed convection parameter λ, concentration buoyancy parameter N, heat transfer

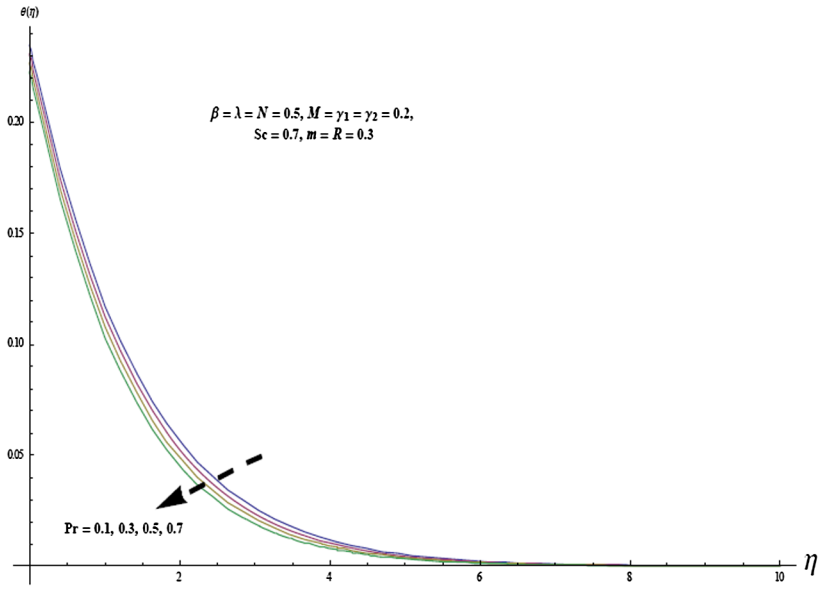

Figure 12 Variation of Pr on $\theta(\eta)$.

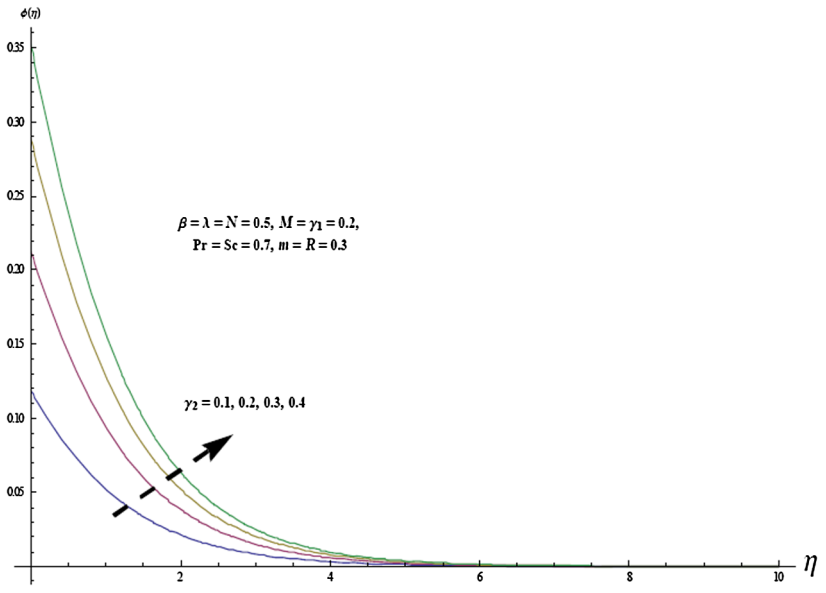

Figure 13 Variation of γ_2 on $\varphi(\eta)$.

Biot number γ_1, mass transfer Biot number γ_2 and radiation parameter R. Numerical values of the skin friction coefficients, local Nusselt number and Sherwood number decrease with an increase in Casson parameter β. For assisting flow ($\lambda > 0$), local Nusselt number and Sherwood numbers enhance when N increases. The skin friction coefficients reduce for larger N, and opposite behavior is noted in the case of opposing flow ($\lambda < 0$). Sherwood number and transversal skin friction coefficient are increased with an increase in Biot number γ_2, while skinfriction coefficient and local Nusselt number decrease with an increase in γ_2.

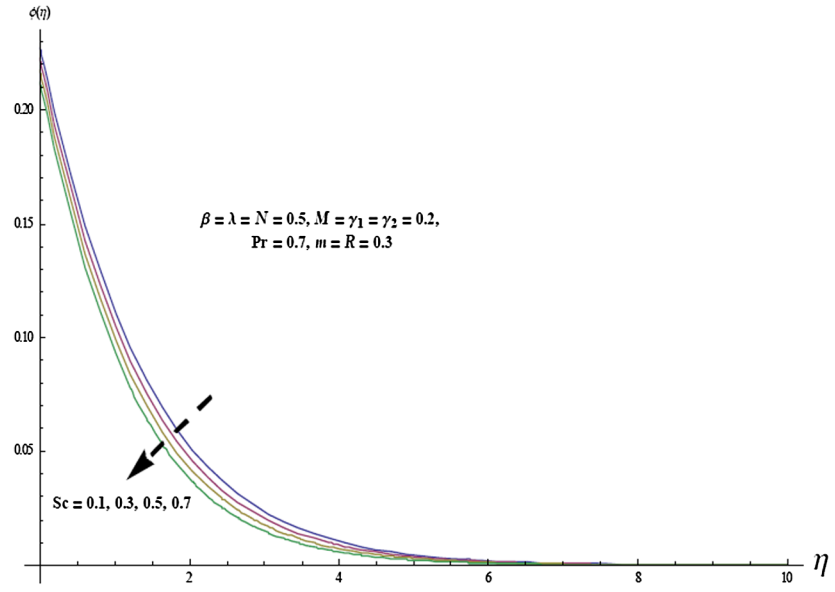

Figure 14 Variation of Sc on $\varphi(\eta)$.

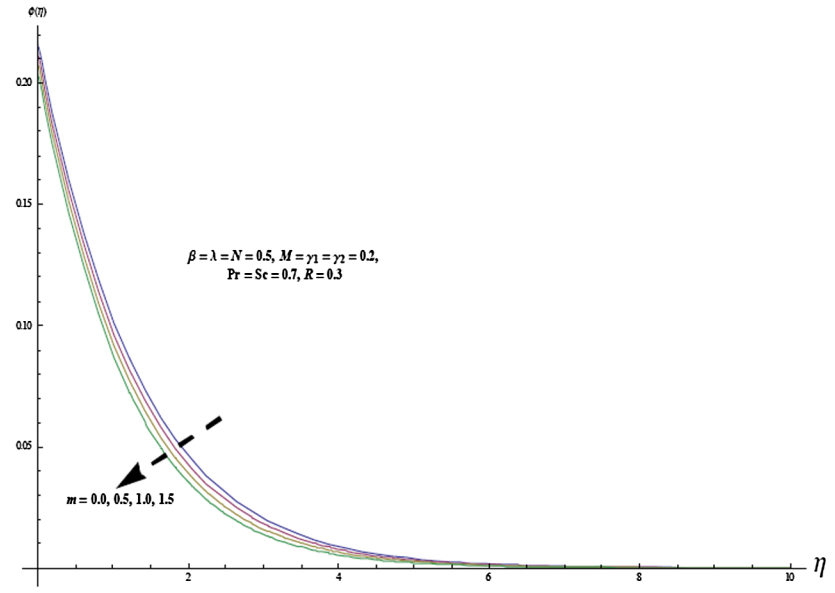

Figure 15 Variation of m on $\varphi(\eta)$.

5 Conclusions

The present study inspected the MHD mixed convection flow over a stretching surface with thermal radiation and Hall effects. Casson fluid model is recycled as a non-Newtonian fluid. Key facts of the current study are as follows:

(a) Momentum boundary layer thickness and the velocity profile $f'(\eta)$ decline for higher values of M and m.

Table 2 Mathematical values of physical constraints at the boundaries for altered values of factors β, R, M, γ_1, γ_2 when $m = 0.5$, Pr = 1.0, Sc = 0.7 and $\hbar_f = \hbar_h = \hbar_\theta = \hbar_\varphi = -0.3$

β	M	λ	N	γ_1	γ_2	R	$-(1+\frac{1}{\beta})f''(0)$	$(1+\frac{1}{\beta})h'(0)$	$-\theta'(0)$	$-\varphi'(0)$
0.3	0.2	0.3	0.3	0.2	0.2	0.3	2.0819	0.10957	0.14801	0.14777
0.5							1.7240	0.093799	0.14659	0.14645
0.7							1.4865	0.086024	0.14534	0.14569
0.5	0.2						1.7240	0.093799	0.14660	0.14670
	0.5						1.8292	0.22869	0.14613	0.14614
	0.8						1.9390	0.35670	0.14560	0.14556
0.5	0.2	−0.3					1.8792	0.092367	0.14594	0.14574
		0.0					1.8005	0.093237	0.14628	0.14596
		0.5					1.6743	0.094184	0.14679	0.14656
0.5	0.2	0.3	0.0				1.7416	0.093717	0.14653	0.14590
			0.3				1.7240	0.093775	0.14660	0.14610
			0.6				1.7065	0.093952	0.14667	0.14640
0.5	0.2	0.3	0.3	0.2			1.7240	0.093775	0.14660	0.14610
				0.5			1.6789	0.094190	0.26222	0.14667
				0.7			1.6610	0.094277	0.30859	0.14701
0.5	0.2	0.3	0.3	0.2	0.3		1.7183	0.093792	0.14661	0.19390
					0.5		1.7102	0.093829	0.14664	0.26108
					0.7		1.7047	0.093841	0.14668	0.30757
0.5	0.2	0.3	0.3	0.2	0.2	0.0	1.7391	0.093643	0.15413	0.14624
						0.3	1.7240	0.093720	0.14659	0.14639
						0.6	1.7098	0.093855	0.14038	0.14651

(b) In the situation of assisting flow ($\lambda > 0$), both the velocity profile $f'(\eta)$ and momentum boundary layer thickness are increase, while opposite performance is perceived in the case of opposing flow ($\lambda < 0$).

(c) Transversal velocity $h(\eta)$ upsurges with an upturn in Hartman number M and concentration buoyancy constraint N, while it declines with an upturn in Hall restriction m.

(d) Thermal boundary layer thickness improves with an upsurge in Biot number γ_1 and thermal radiation factor R, while it lessens for superior Pr.

(e) Skin friction quantity, transversal skin friction coefficient, local Nusselt and Sherwood numbers are compact for greater Casson fluid parameter β.

(f) In the case of assisting flow ($\lambda > 0$), the skin friction coefficient reduces, although opposite performance for opposing flow ($\lambda < 0$) is perceived.

(g) Skin friction coefficient declines with a rise in concentration buoyancy factor N, while transversal skin resistance number, local Nusselt and Sherwood records drop.

(h) Local Nusselt and Sherwood figures upsurge for larger Biot quantities γ_1 and γ_2.

Acknowledgements
This work was partially supported by the Deanship of Scientific Research (DSR), King Abdulaziz University, Jeddah, Saudi Arabia.

Competing interests
The authors declare that there is no competing interest.

Authors' contributions
All authors contributed equally to the manuscript and approved the final manuscript.

Author details
[1]Department of Mathematics, COMSATS Institute of Information Technology, Wah Cantt., 47040, Pakistan. [2]Department of Mathematics, Quaid-i-Azam University, 45320, Islamabad, 44000, Pakistan. [3]Nonlinear Analysis and Applied Mathematics (NAAM) Research Group, Faculty of Science, King Abdulaziz University, P.O. Box 80203, Jeddah, 21589, Saudi Arabia.

Publisher's Note

Received: 4 January 2017 Accepted: 2 May 2017 Published online: 20 September 2017

References

1. Gupta, AS: Hydromagnetic flow past a porous flat plate with Hall effects. Acta Mech. **22**, 281-287 (1975)
2. Hayat, T, Abbas, Z, Asghar, S: Effects of Hall current and heat transfer on rotating flow of a second grade fluid through a porous medium. Commun. Nonlinear Sci. Numer. Simul. **13**, 2177-2192 (2008)
3. Saleem, AM, Aziz, MAE: Effect of Hall currents and chemical reaction on hydromagnetic flow of a stretching vertical surface with internal heat generation/absorption. Appl. Math. Model. **32**, 1236-1254 (2008)
4. Aziz, MAE, Nabil, T: Homotopy analysis solution of hydromagnetic mixed convection flow past an exponentially stretching sheet with Hall current. Math. Probl. Eng. **2012**, 454023 (2012)
5. Pal, D: Hall current and MHD effects on heat transfer over an unsteady stretching permeable surface with thermal radiation. Comput. Math. Appl. **66**, 1161-1180 (2013)
6. Crane, LJ: Flow past a stretching plate. Z. Angew. Math. Phys. **21**, 645-647 (1970)
7. Eldabe, NTM, Salwa, MGE: Heat transfer of MHD non-Newtonian Casson fluid flow between two rotating cylinders. J. Phys. Soc. Jpn. **64**, 41-64 (1995)
8. Mukhophadhyay, S: Casson fluid flow and heat transfer over a nonlinearly stretching surface. Chin. Phys. B **22**, 074701 (2013)
9. Shehzad, SA, Hayat, T, Qasim, M, Asghar, S: Effects of mass transfer on MHD flow of a Casson fluid with chemical reaction and suction. Braz. J. Chem. Eng. **30**, 187-195 (2013)
10. Mukhophadhyay, S, Vajravelu, K: Diffusion of chemically reactive species in Casson fluid flow over an unsteady permeable stretching surface. J. Hydrodyn. **25**, 591-598 (2013)
11. Makinde, OD, Sibanda, P: Magnetohydrodynamic mixed convective flow and heat and mass transfer past a vertical plate in a porous medium with constant wall suction. J. Heat Transf. **130**, 112602 (2008)
12. Turkyilmazoglu, M: The analytical solution of mixed convection heat transfer and fluid flow of a MHD viscoelastic fluid over a permeable stretching surface. Int. J. Mech. Sci. **77**, 263-268 (2013)
13. Alsaadi, FE, Shehzad, SA, Hayat, T, Monaquel, SJ: Soret and Dufour effects on the unsteady mixed convection flow over a stretching surface. J. Mech. **29**, 623-632 (2013)
14. Siegel, R, Howell, JR: Thermal Radiation Heat Transfer. Hemisphere, Washington (1993)
15. Modest, MF: Radiative Heat Transfer. Elsevier, Amsterdam (2003)
16. Mukhopadhyay, S: Effect of thermal radiation on unsteady mixed convection flow and heat transfer over a porous stretching surface in porous medium. Int. J. Heat Mass Transf. **52**, 3261-3265 (2009)
17. Turkyilmazoglu, M: Thermal radiation effects on the time-dependent MHD permeable flow having variable viscosity. Int. J. Therm. Sci. **50**, 88-96 (2011)
18. Shehzad, SA, Alsaedi, A, Hayat, T: Influence of thermophoresis and Joule heating on the radiative flow of Jeffery fluid with mixed convection. Braz. J. Chem. Eng. **30**, 897-908 (2013)
19. Aziz, A: A similarity solution for thermal boundary layer over a flat plate with a convective surface boundary condition. Commun. Nonlinear Sci. Numer. Simul. **14**, 1064-1068 (2009)
20. Makinde, OD, Aziz, A: MHD mixed convection from a vertical plate embedded in a porous medium with a convective boundary condition. Int. J. Therm. Sci. **49**, 1813-1820 (2010)
21. Shehzad, SA, Alsaedi, A, Hayat, T: Three-dimensional flow of Jeffery fluid with convective surface boundary conditions. Int. J. Heat Mass Transf. **55**, 3971-3976 (2012)
22. Makinde, OD, Aziz, A: Boundary layer flow of a nanofluid past a stretching sheet with a convective boundary condition. Int. J. Therm. Sci. **50**, 1326-1332 (2011)
23. Liu, YP, Liao, SJ, Li, ZB: Symbolic computation of strongly nonlinear periodic oscillations. J. Symb. Comput. **55**, 72-95 (2013)
24. Hayat, T, Shehzad, SA, Ashraf, MB, Alsaedi, A: Magnetohydrodynamic mixed convection flow of thixotropic fluid with thermophoresis and Joule heating. J. Thermophys. Heat Transf. **27**, 733-740 (2013)
25. Abbasbandy, S, Hashemi, MS, Hashim, I: On convergence of homotopy analysis method and its application to fractional integro-differential equations. Quaest. Math. **36**, 93-105 (2013)
26. Zheng, L, Niu, J, Zhang, X, Gao, Y: MHD flow and heat transfer over a porous shrinking surface with velocity slip and temperature jump. Math. Comput. Model. **56**, 133-144 (2012)
27. Rashidi, MM, Rajvanshi, SC, Keimanesh, M: Study of pulsatile flow in a porous annulus with the homotopy analysis method. Int. J. Numer. Methods Heat Fluid Flow **22**, 971-989 (2012)
28. Rashidi, MM, Kavyani, N, Abelman, S: Investigation of entropy generation in MHD and slip flow over a rotating porous disk with variable properties. Int. J. Heat Mass Transf. **70**, 892-917 (2014)
29. Turkyilmazoglu, M: Solution of Thomas-Fermi equation with a convergent approach. Commun. Nonlinear Sci. Numer. Simul. **17**, 4097-4103 (2012)
30. Ramzan, M, Farooq, M, Alsaedi, A, Hayat, T: MHD three-dimensional flow of couple stress fluid with Newtonian heating. Eur. Phys. J. Plus **128**, 49 (2013)